JOURNAL OF MATERIALS SCIENCE 32 (1997) 1781–1788

# The creep–rupture properties and the initiation and growth of the grain-boundary cracks in the cobalt-base HS-21 alloy

M. TANAKA
*Department of Mechanical Engineering, Mining College, Akita University, 1-1, Tegatagakuen-cho, Akita 010, Japan*

The effect of the grain-boundary microstructures on the creep–rupture properties and the initiation and growth of the grain-boundary cracks was investigated using four kinds of specimen of various grain-boundary microstructures in the cobalt-base HS-21 alloy at 1089 K in air. Both the rupture strength and the creep ductility increased with increasing mean value of the fractal dimension of the grain boundaries, $D_{gb}$. The strain to crack initiation was largest in the specimen of the highest $D_{gb}$ value (1.241), while the strain was much the same in the specimens of the $D_{gb}$ value less than 1.162. This was explained by the local variation in the grain-boundary microstructures in these specimens. The mean value of the fractal dimension of the grain-boundary fracture, $D_f$, was close to the value of $D_{gb}$, although the value of $D_f$ was a little higher than that of $D_{gb}$ in the specimens of the lower $D_{gb}$ values. The fracture appearance changed from a brittle grain-boundary fracture to a ductile one with increasing values of $D_{gb}$ and $D_f$. The crack-growth rate is the surface-notched specimens decreased with increasing value of $D_{gb}$. The threshold stress intensity factor for crack growth was higher in the specimens with the higher $D_{gb}$ values.

## 1. Introduction

It is known that serrated grain boundaries are effective in improving the creep–rupture properties in many heat-resistant steels and alloys [1–8]. As Ashby and co-workers [9–11] revealed, serrated grain boundaries composed of grain-boundary ledges, bumps and curvature, retard the grain-boundary sliding, which leads to the initiation and growth of the grain-boundary microcracks at high temperatures. Yamamoto *et al.* [5] and Tanaka and co-workers [6–8] have also shown that the grain-boundary fracture surface of the specimen with serrated grain boundaries is a ductile fracture surface composed of grain-boundary steps, ledges and small dimples, while the fracture surface of the specimen with straight grain boundaries is a typical brittle grain-boundary fracture surface. However, it has been difficult, until recently, to describe quantitatively the grain-boundary microstructures and fracture surfaces because of their complexity.

Mandelbrot *et al.* [12] first revealed the fractal nature (self-similarity) of fracture surfaces in the impact-loaded and fractured specimens of steels. As Milman *et al.* [13] have recently reviewed, the concept of the fractal geometry developed by Mandelbrot [14] as well as the measurement techniques of the fractal dimension have been applied to the morphological analysis of fracture surfaces in metallic materials, glasses and ceramics. The concept of the fractal geometry has been applied [15, 16] to creep fracture and it was found that there is a correlation between the fractal dimension of the grain-boundary fracture (the fractal dimension of the grain-boundary fracture surface profile in the two-dimensional section, $D'_f$, $1 < D'_f < 2$) and the creep–rupture properties in the heat-resistant alloys. The creep–rupture properties can also be correlated to the fractal dimension of the grain boundaries (the fractal dimension of the grain-boundary surface profile in the two-dimensional section, $D'_{gb}$, $1 < D'_{gb} < 2$) [17].

Gokhale and co-workers [18, 19] have discussed the experimental techniques for the estimation of the fractal dimension of fracture surfaces. They have also pointed out as a result of a statistical analysis that thorough profile sampling is required to achieve precision in determining the fractal dimension for inhomogeneous surfaces [19]. However, the local variation in the microstructures or in the fracture surface morphologies can be correlated to critical phenomena like the fracture initiation in the specimens, while the overall fracture process may be governed by the averaged microstructures.

The initiation and growth of the grain-boundary cracks, which is related to the creep–rupture properties, may depend on the ruggedness of grain boundaries or fracture surface structures in the materials. In this study, the effect of the grain-boundary microstructures on the creep-rupture properties and the initiation and growth of the grain-boundary cracks was investigated using four kinds of specimen with various grain-boundary morphologies in the cobalt-base

0022–2461  

HS-21 alloy at 1089 K in air. The mean values of the fractal dimensions of the grain boundaries and of the grain-boundary fracture and their standard deviations were estimated in the scale range of the fractal analysis less than one grain-boundary length by the box-counting method [14, 20, 21]. The relationship between the creep–rupture properties, the initiation and growth of the grain-boundary cracks and these fractal dimensions in the HS-21 alloy was then discussed.

## 2. Experimental procedure

### 2.1. Materials and creep and creep–rupture experiments

Table I shows the chemical composition of the commercial wrought cobalt-base HS-21 alloy. The alloy bars of 16 mm diameter were heat-treated to obtain four kinds of specimen with different grain-boundary configuration while keeping the strength of the matrix almost constant. Table II shows the heat treatments, the mean value, $D_{gb}$, and the standard deviation, $s_{gb}$, of the fractal dimension of the grain boundaries, and the matrix hardness in the specimens of the HS-21 alloy. The grain diameter of these specimens, $d_g$, was 130 μm. The fractal dimension of the grain boundaries is defined as that of the grain-boundary surface profile in the two-dimensional section ($1 < D_{gb} < 2$). As will be shown later, the values of $D_{gb}$ and $s_{gb}$ were estimated on five grain boundaries in each specimen by the box-counting method in this study [14, 20, 21]. The range of fractal dimension is also shown in Table II.

Fig. 1 shows the optical micrographs of the heat-treated specimens of the HS-21 alloy. Large $M_{23}C_6$ type carbide particles are visible in the specimens of the higher $D_{gb}$ values (Fig. 1c and d), while fine $M_{23}C_6$ precipitates can be observed in the grains (Fig. 1a–d [8]. Grain boundaries are considerably serrated in specimens of the higher $D_{gb}$ values (Fig. 1c and d), whereas they are almost straight in specimens of lower $D_{gb}$ values. The heat-treated specimens were machined into creep specimens as shown in Fig. 2. Smooth, round, bar specimens of 5 mm diameter, $d$, and 30 mm gauge length were used for creep–rupture experiments (Fig. 2a), and those with a shallow transverse notch were employed for crack-growth experiments (Fig. 2b). Creep experiments were carried out using single lever-type creep–rupture equipment under the initial creep stresses of 88.2–176 MPa at 1089 K. Conditions of the creep–rupture experiment were chosen to cause grain-boundary fracture in all the specimens. The time to crack initiation was also examined on the smooth, round, bar specimens.

The surface crack length, $l$, of the surface-notched specimen was measured by examining the specimen surface using an optical microscope after interrupting creep tests and cooling the specimens to room temperature. The specimens were heated to the test temperature and were loaded again after the crack-length measurement. The creep stress of the notched specimens is shown by the gross stress, $\sigma_g$, in this study. According to the previous study [22], the geometry of a crack could be known from heat tinting of the smooth, round, bar specimens ruptured at 1089 K. The crack depth, $a$, of the surface-notched specimens could also be known from the surface-crack length, $l$, and the crack geometry. The size of the surface-crack length and crack depth includes that of the notched part. The crack-growth rate was obtained by plotting crack depth, $a$, against time, $t$, and reading the slope of the plotted curve.

### 2.2. Estimation of the fractal dimensions of the grain-boundary fracture and of the grain boundaries

The smooth bar specimens, ruptured under one creep stress (108 MPa), were longitudinally sectioned in the

TABLE I Chemical composition of the cobalt-base HS-21 alloy used in this study (wt %)

| Alloy | C | Cr | Ni | Fe | Mn | Mo | Si | S | P | B | Co |
|---|---|---|---|---|---|---|---|---|---|---|---|
| HS-21 | 0.27 | 26.71 | 2.37 | 0.09 | 0.64 | 5.42 | 0.59 | 0.007 | < 0.005 | 0.003 | Bal. |

TABLE II The heat treatments, the mean value, $D_{gb}$, and the standard deviation, $s_{gb}$, of the fractal dimension of the grain boundaries, and the matrix hardness in the specimens of the HS-21 alloy

| Heat treatments[a] | $D_{gb}$, $s_{gb}$ (range of the fractal dimension) | Matrix hardness (Vickers hardness number, load = 4.9 N) |
|---|---|---|
| 1523 K − 3.6 ks → WQ + 1089 K − 10.8 ks → AC | 1.056, 0.0112 (1.039–1.066) | 418 |
| 1523 K − 3.6 ks → AC + 1089 K − 10.8 ks → AC | 1.107, 0.0194 (1.085–1.136) | 407 |
| 1523 K − 3.6 ks − FC → 1383 K → WQ + 1089 K − 10.8 ks → AC | 1.162, 0.0361 (1.117–1.211) | 419 |
| 1523 K − 3.6 ks − FC → 1323 K → WQ + 1089 K − 10.8 ks → AC | 1.241, 0.0325 (1.208–1.288) | 405 |

[a] WQ = water quenched; AC = air cooled; FC = furnace cooled.

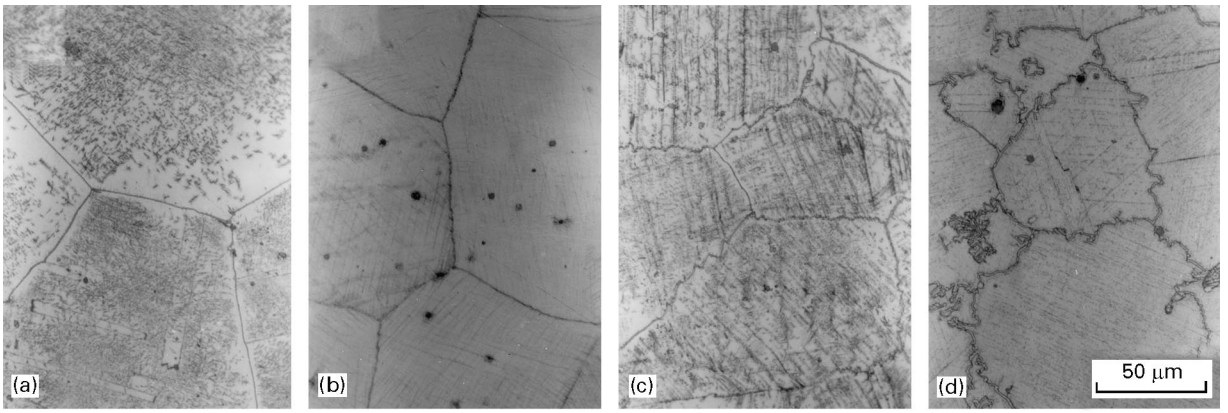


*Figure 1* Optical micrographs of the heat-treated specimens of the HS-21 alloy. (a) $D_{gb} = 1.056$, (b) $D_{gb} = 1.107$, (c) $D_{gb} = 1.162$, (d) $D_{gb} = 1.241$.

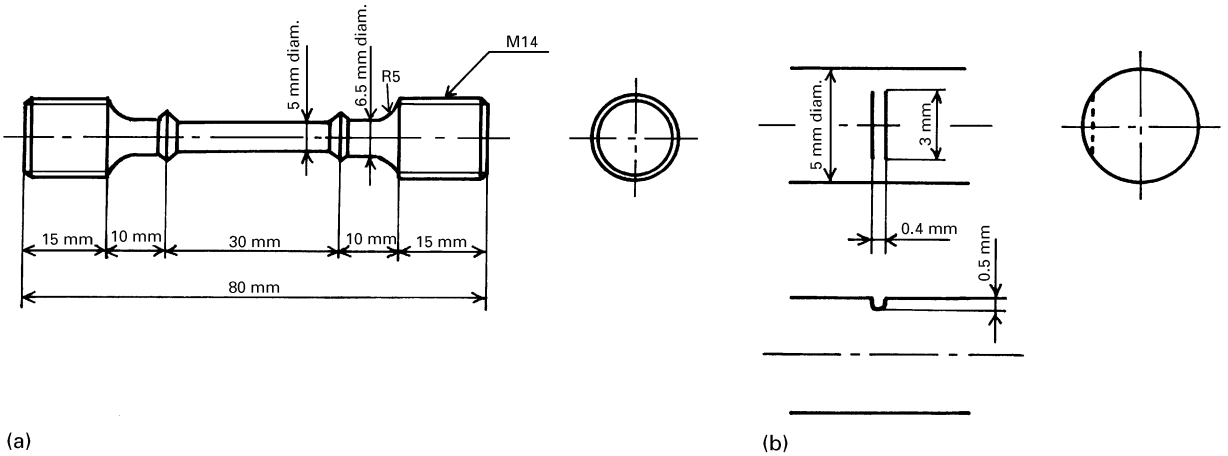


*Figure 2* The geometry of the creep and creep-rupture specimens. (a) Smooth, round, bar specimen; (b) detail of the notched part of the surface-notched specimen.

plane involving the specimen axis, and the fracture surface profiles of five grain boundaries near the specimen axis were examined on each specimen. As well as in the measurement of the fractal dimension of the grain boundaries, $D_{gb}$, four representative photographs of the grain-boundary fracture surface profile were taken using an optical microscope at 400 times or using a scanning electron microscope at 2000 times. The mean value, $D_f$, and the standard deviation, $s_f$, of the fractal dimension of the grain-boundary fracture were estimated on five grain-boundary facets. The fractal dimension of the grain-boundary fracture in this study is the fractal dimension of the grain-boundary fracture surface profile in the two-dimensional section ($1 < D_f < 2$) estimated in the scale range, $r$, smaller than one grain-boundary length ($6.7 \times 10^{-7}$ m $\leqslant r \leqslant 1.3 \times 10^{-6}$ m, $5.2 \times 10^{-3} \leqslant r/d_g \leqslant 0.10$). The fractal dimension of the grain boundaries, $D_{gb}$, was also estimated in the similar scale range ($4.4 \times 10^{-3} \leqslant r/d_g \leqslant 8.8 \times 10^{-2}$).

Fig. 3 shows a schematic illustration of the box-counting method applied to the estimation of the fractal dimensions of the grain-boundary fracture and of the grain boundaries. The value of $N_i$ is the number of boxes of the side length, $r$, which intersect the $i$th profile of the grain-boundary facet (or the $i$th profile of the grain-boundary surface). The length of the $i$th profile of the grain-boundary facet (or the $i$th profile of the grain-boundary surface), $L_i$, is given by a product

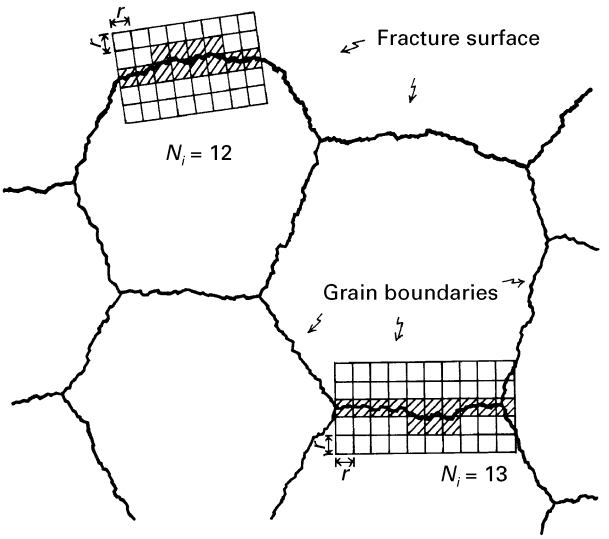


*Figure 3* Schematic illustration of the box-counting method applied to the estimation of the fractal dimensions of the grain-boundary fracture and of the grain boundaries.

of $N_i$ and $r$, such that $L_i = N_i r$. The length of the $i$th profile, $L_i$, is generally correlated to the scale length of the fractal analysis, $r$, by the following equation [14, 20, 21, 23]

$$L_i = L_{i\,0}\, r^{1-D_i} \tag{1}$$

where $D_i$ is the fractal dimension of the $i$th profile and $L_{i\,0}$ is a constant. The value of $D_i$ can be obtained by fitting the experimental data of the $i$th profile to the above equation. The mean value, $D$, and the standard deviation, $s$, of the fractal dimension are given by

$$D = \sum_{i=1}^{n} D_i/n \tag{2}$$

$$s = \left[\sum_{i=1}^{n} (D_i - D)^2/(1-n)\right]^{1/2} \tag{3}$$

where $D = D_i$ and $s = s_f$ for the fractal dimension of the grain-boundary fracture, and $D = D_{gb}$ and $s = s_{gb}$ for the fractal dimension of the grain boundaries, and $n = 5$ in this study.

## 3. Results and discussion

### 3.1. Effects of grain-boundary configuration on the creep–rupture properties of smooth, round, bar specimens

Fig. 4 shows the rupture lives of the specimens in the HS-21 alloy at 1089 K. The rupture lives of the specimens tend to increase with increasing the mean value of the fractal dimension of the grain boundaries, $D_{gb}$. The increase in the value of $D_{gb}$ leads to a large improvement of the rupture lives, especially under the higher stresses.

Fig. 5 shows the creep ductility of the specimens in the HS-21 alloy. Both the elongation and the reduction of area increase with increasing the value of $D_{gb}$. Thus, the improvement of the creep–rupture properties by serrated grain boundaries depend on the value of $D_{gb}$. The change in the creep–rupture properties with the value of $D_{gb}$ can be explained by the initiation and growth of the grain–boundary crack during creep.

Fig. 6 shows examples of creep curves of the specimens of the HS-21 alloy tested under a stress of 108 MPa at 1089 K. The first grain-boundary crack seems to initiate on the specimen surface. The strain to crack initiation is also shown in this figure. As reported in the previous study [8], the creep curves of the HS-21 alloy have a long tertiary creep regime and a very short steady-state creep regime in the temperature range 1089–1311 K. The strain to the initiation of the surface crack is about 0.0083 in the specimen of $D_{gb} = 1.241$, whereas it is almost the same (about 0.0052–0.0056) in the specimens of $D_{gb}$ less than 1.162.

Ashby and co-workers [9–11] discussed the influence of ledges, bumps, curvature, particles or precipitates on the grain-boundary sliding. Obviously, all these make the grain-boundary sliding difficult and increase the value of $D_{gb}$ as well. According to the previous study [6, 7], serrated grain boundaries (with high $D_{gb}$ value) are effective in retarding the initiation of the grain-boundary cracks controlled by grain-boundary sliding, and the strain to crack initiation is larger in the specimen with serrated grain boundaries (with high $D_{gb}$ value) compared with the one with straight grain boundaries (with low $D_{gb}$ value). Therefore, the strain to crack initiation is the largest in the specimen of the largest $D_{gb}$ value. However, there is almost no difference in the strain to crack initiation between the specimens of $D_{gb}$ less than 1.162. This can be explained by boundary to boundary variation in

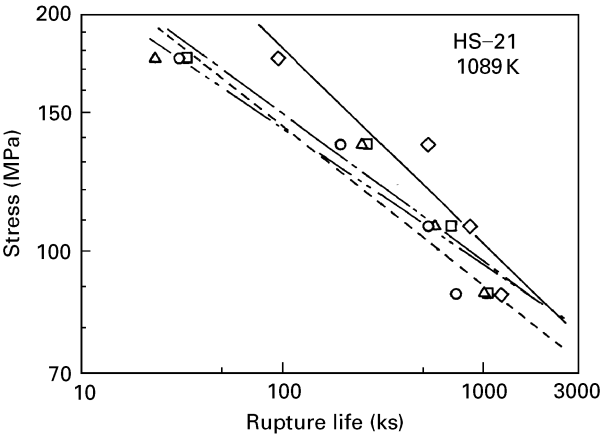


*Figure 4* The rupture lives of the specimens in the HS-21 alloy at 1089 K, for the $D_{gb}$ values: (–○–) 1.056, (--△--) 1.107, (––□––) 1.162, (—◇—) 1.241.

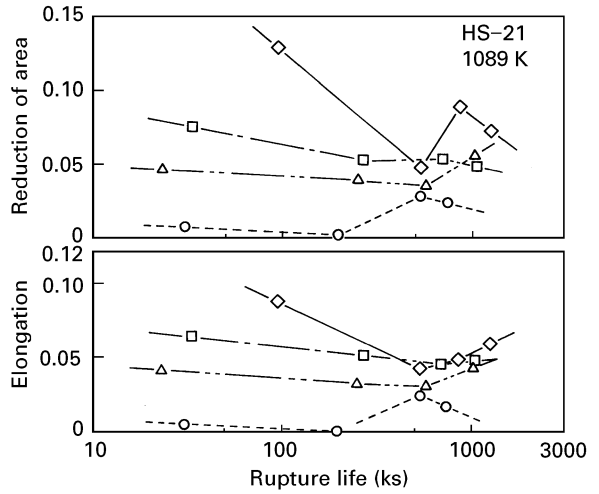


*Figure 5* The creep ductility of the specimens in the HS-21 alloy at 1089 K. Values of $D_{gb}$ given in Fig. 4.

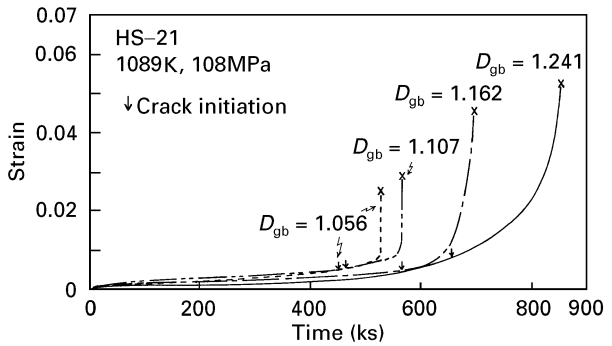


*Figure 6* Creep curves of the specimens in the HS-21 alloy tested under a stress of 108 MPa at 1089 K.

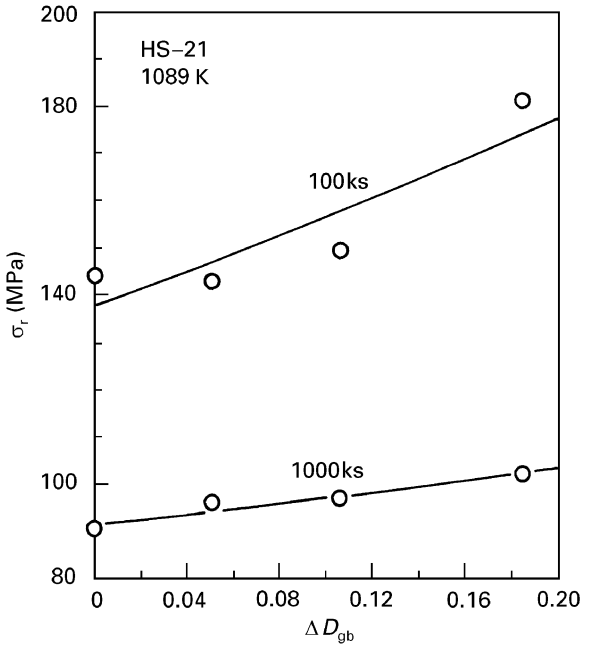


*Figure 7* The relationship between the rupture strength, $\sigma_r$, and the increment in the mean value of the fractal dimension of the grain boundaries, $\Delta D_{gb}$, in the HS-21 alloy at 1089 K ($\Delta D_{gb} = D_{gb} - 1.056$).

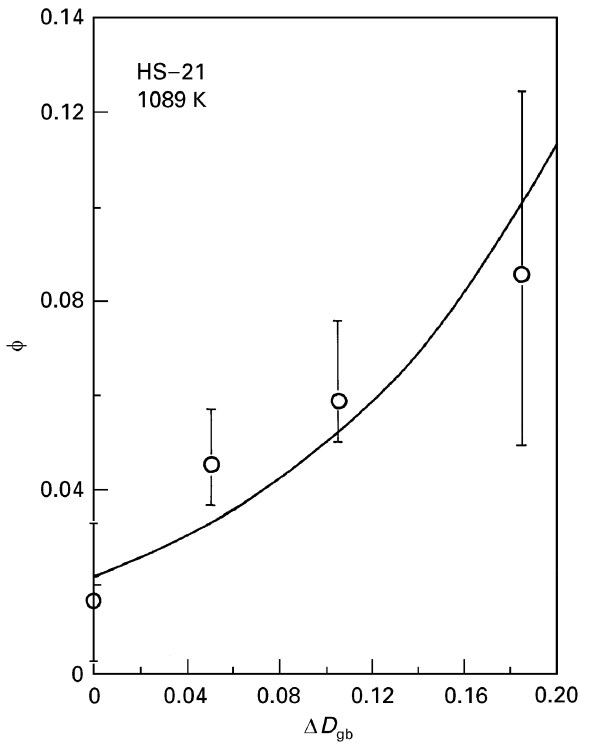


*Figure 8* The relationship between the reduction of area, $\phi$, and the increment in the mean value of the fractal dimension of the grain boundaries, $\Delta D_{gb}$, in the HS-21 alloy at 1089 K ($\Delta D_{gb} = D_{gb} - 1.056$).

the fractal dimension of the grain boundaries in the specimens indicated by the standard deviation, $s_{gb}$, and the range of the fractal dimension (Table II). The crack initiation may be associated with the straighter grain boundaries (with the lower $D_{gb}$ values) in the same specimen, although this was not confirmed in each specimen. As indicated by the value of $s_{gb}$ (Table II), the local variation of the fractal dimension seems to increase up to $D_{gb} = 1.162$. It is deduced that the lowest value of the fractal dimension in the specimen of $D_{gb} = 1.107$ and in the specimen of $D_{gb} = 1.162$ is close to that of the fractal dimension in the specimen of $D_{gb} = 1.056$, while there is a large difference in the lowest value of the fractal dimension between the specimen of $D_{gb} = 1.241$ and the specimen of $D_{gb} = 1.056$. Thus, the crack initiation may be associated not with the mean value of the fractal dimension of the grain boundaries, $D_{gb}$, but with the local variation of the fractal dimension in the specimens.

Fig. 7 shows the relationship between the rupture strength, $\sigma_r$, and the increment in the mean value of the fractal dimension of the grain boundaries, $\Delta D_{gb}$, in the HS-21 alloy at 1089 K ($\Delta D_{gb} = D_{gb} - 1.056$). The value of $\sigma_r$ increases with increase of the value of $\Delta D_{gb}$, and the increase of $\sigma_r$ with $\Delta D_{gb}$ is more remarkable at the shorter rupture life (100 ks). Fig. 8 shows the relationship between the reduction of area, $\phi$, and the increment in the mean value of the fractal dimension of the grain boundaries, $\Delta D_{gb}$, in the HS-21 alloy at 1089 K. The data points indicate the averaged values of the reduction of area over four creep stresses, and the ranges of the values are also shown in this figure. The reduction of area also increases with increasing value of $D_{gb}$. Similar results were obtained on the dependence of the elongation on the value of $D_{gb}$. These results can be correlated to the fracture mode in the specimens.

Fig. 9 shows the microstructures of the specimens in the HS-21 alloy ruptured under a stress of 108 MPa at 1089 K. The tensile direction is vertical in the optical micrographs. Long grain-boundary cracks are observed near the fracture surface in the specimens of the smaller values of $D_{gb}$ (Fig. 9a, b), while shorter grain-boundary cracks can be seen in the specimens of the larger values of $D_{gb}$ (Fig. 9c and d). The fracture surface of the specimen of the lowest $D_{gb}$ value (1.056) is a typical brittle grain-boundary facet (Fig. 9e), whereas that of the specimen of the highest $D_{gb}$ value (1.241) is a ductile grain-boundary fracture surface composed of ledges, steps and small dimples (Fig. 9h). The fracture surfaces of the specimens of the intermediate value of $D_{gb}$ have a mixed microstructure of brittle and ductile fracture surfaces (Fig. 9f and g), which reflect the local variation of the fractal dimension of the grain boundaries in these specimens (Table II), and the area fraction of the ductile grain-boundary fracture surface is larger in the specimen of the higher $D_{gb}$ value (Fig. 9g).

Table III shows the mean value, $D_f$, and the standard deviation, $s_f$, of the fractal dimension of the grain-boundary fracture and the range of the fractal dimension in the specimens of various $D_{gb}$ values ruptured under a stress of 108 MPa at 1089 K. The value of $D_f$ is close to that of $D_{gb}$, although it is a little higher than that of $D_{gb}$ in the specimens of the lower $D_{gb}$ values. The value of $s_f$ is also close to that of $s_{gb}$ in these specimens (Table II). The fracture appearance changes from a brittle grain-boundary fracture to a ductile one with increasing value of $D_f$ (and the value of $D_{gb}$). It seems that the brittle to ductile transition in

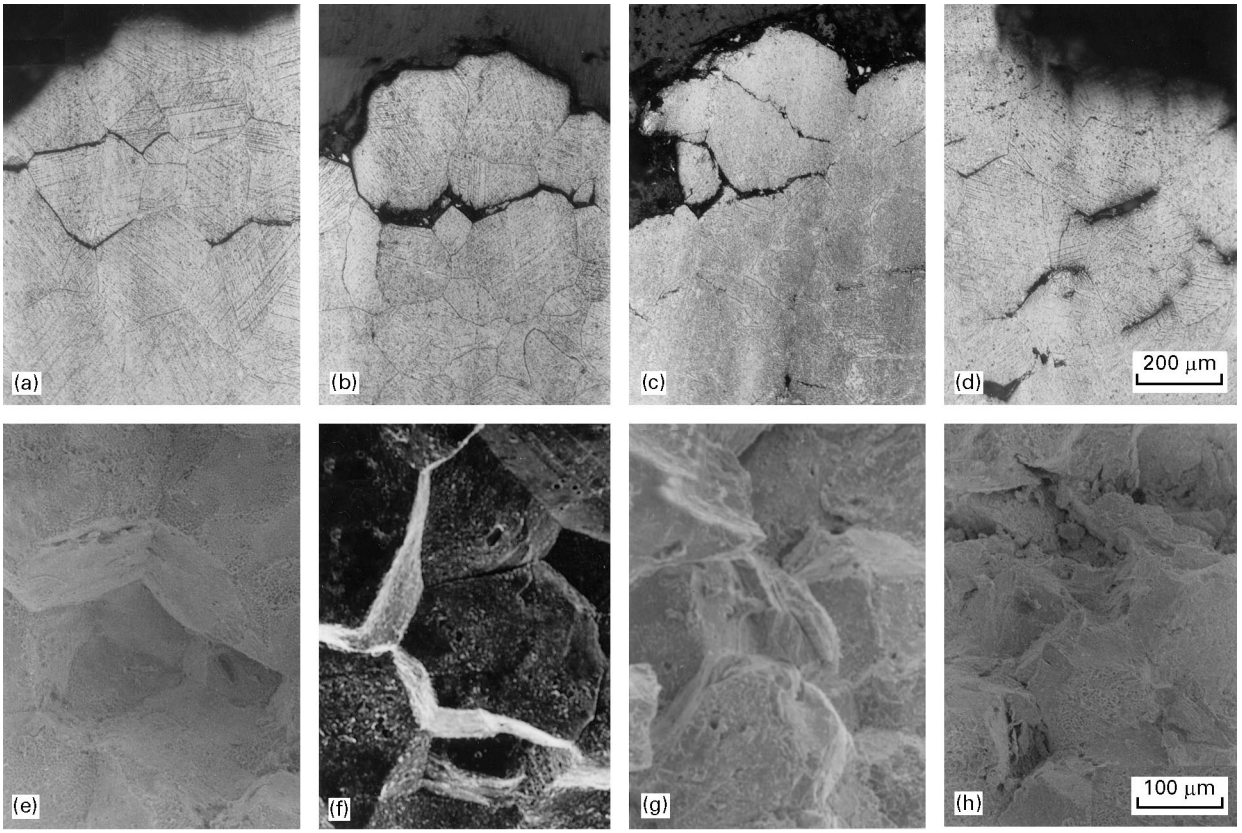


*Figure 9* The microstructures of the specimens in the HS-21 alloy ruptured under a stress of 108 MPa at 1089 K. (a, e) $D_{gb} = 1.056$, (b, f) $D_{gb} = 1.107$, (c, g) $D_{gb} = 1.162$, (d, h) $D_{gb} = 1.241$.

TABLE III The mean value, $D_f$, and the standard deviation, $s_f$, of the fractal dimension of the grain-boundary fracture in the specimens of various $D_{gb}$ values of the HS-21 alloy ruptured under the stress of 108 MPa at 1089 K

| $D_{gb}$ | $D_f$, $s_f$ (range of the fractal dimension) |
|---|---|
| 1.056 | 1.124, 0.0171 (1.099–1.139) |
| 1.107 | 1.152, 0.0213 (1.126–1.179) |
| 1.162 | 1.216, 0.0358 (1.182–1.271) |
| 1.241 | 1.261, 0.0307 (1.212–1.289) |

the fracture appearance occurs at the fractal dimension of the grain-boundary fracture of about 1.15–1.20 (at that of the grain boundaries of about 1.10–1.15). Further, the fracture appearance in the specimens was not changed with creep stress. Thus, both increases in the rupture strength and in the creep ductility with increasing $D_{gb}$ value can be explained by an increase in the area fraction of the ductile grain-boundary fracture indicated by the value of $D_f$ in the HS-21 alloy.

## 3.2. Creep crack growth in the surface-notched specimens

The growth of the grain-boundary crack during creep at 1089 K was investigated using three kinds of specimen with different $D_{gb}$ values (1.056, 1.162 and 1.241). Fig. 10 shows the geometry of the grain-boundary cracks observed on the smooth, round, bar specimens of the HS-21 alloy ruptured at 1089 K. The product of specimen radius, $d/2$, and open angle, $\theta$, gives the surface crack length ($l = d\theta/2$). The ratio of crack depth, $a$, to specimen diameter, $d$, i.e. $a/d$, increases with an increase in the angle $\theta$ (or the surface crack length, $l$), while the ratio $R/d$ shows a constant value of 0.630 for all the specimens of the HS-21 alloy, where $R$ is the radius of curvature at the crack front. The similar value of $R/d$ (0.679) was obtained in the austenitic 21Cr–4Ni–9Mn steel [22]. Thus, if the value of $l$ is known, the value of $a/d$ can be estimated from the angle $\theta$ by using Fig. 10.

Fig. 11 shows the increment of the surface crack length, $\Delta l$, in the surface-notched specimens of the HS-21 alloy during creep at 1089 K. The period of the crack growth is longer in the specimen of the higher $D_{gb}$ value under both gross stresses ($\sigma_g = 73.5$, 88.2 MPa), although the period of the crack growth in the surface-notched specimen is much less than that in the smooth bar specimen (Fig. 6). The time to crack initiation is not always shortest in the surface-notched specimen of the lowest $D_{gb}$ value. This behaviour can be explained as follows. The grain boundary at which a crack is expected to initiate is not always located at the notch root where the stress concentration is the highest [22]. Further, as described in the previous section, there is a boundary-to-boundary variation in the fractal dimension of the grain boundaries. These factors may affect the initiation of the grain-boundary

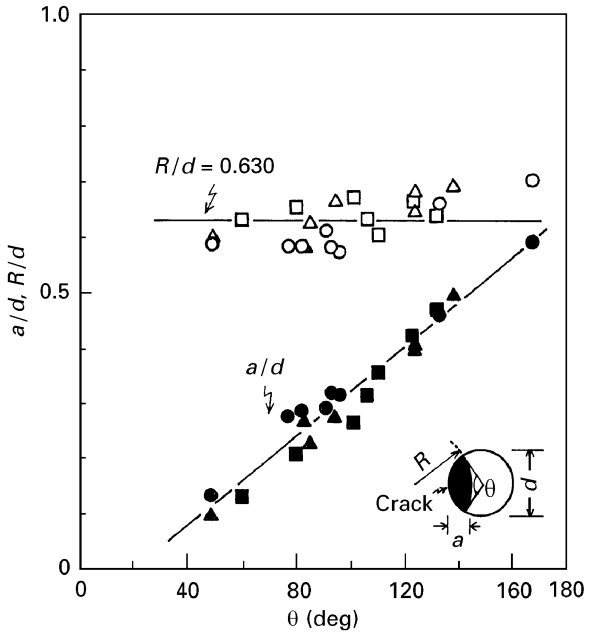


*Figure 10* The geometry of the grain-boundary cracks observed on the smooth, round, bar specimens of the HS-21 alloy ruptured at 1089 K. $D_{gb}$: (△, ▲) 1.056, (□, ■) 1.162, (○, ●) 1.241.

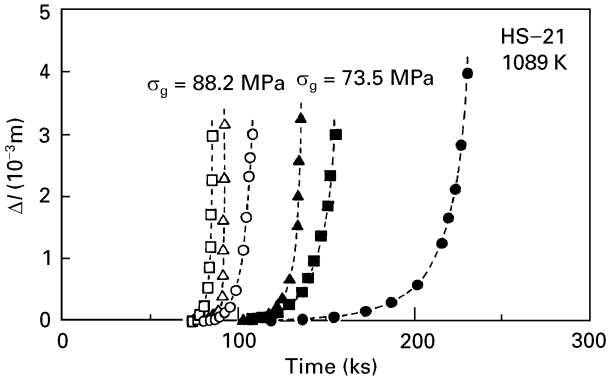


*Figure 11* The increment of the surface crack length, $\Delta l$, with time in the surface-notched specimens of the HS-21 alloy during creep at 1089 K. $D_{gb}$: (△, ▲) 1.056, (□, ■) 1.162, (○, ●) 1.241.

cracks. The change in the notch-opening displacement with time was also measured in the surface-notched specimens during creep at 1089 K, but it is not shown here, because the change in the notch-opening displacement was too small (less than $10^{-5}$ m) to identify through crack-growth experiments because of low creep ductility of the HS-21 alloy.

The crack depth, $a$, and the crack growth rate, d$a$/d$t$, can be obtained from the results of the surface crack-growth experiments using the relationship between crack depth, $a$, and the angle θ (Fig. 10). Fig. 12 shows the relationship between the crack-growth rate, d$a$/d$t$, and the maximum stress intensity factor, $K_I$, in the HS-21 alloy during creep at 1089 K. The $K_I$ values for the surface-notched specimens is given using variables shown in Fig. 12 by Kiuchi *et al.*'s equation [24]

$$K_I = \sigma_g(\pi a)^{1/2}\{1.12 + (0.30/d - 1.85/R)a - [6.63/d^2 - 10.25/(Rd)]a^2 + [23.13/d^3 - 18.75/(Rd^2)]a^3\} \quad (a/d \leqslant 0.4 \text{ and } R \geqslant 0.5d) \quad (4)$$

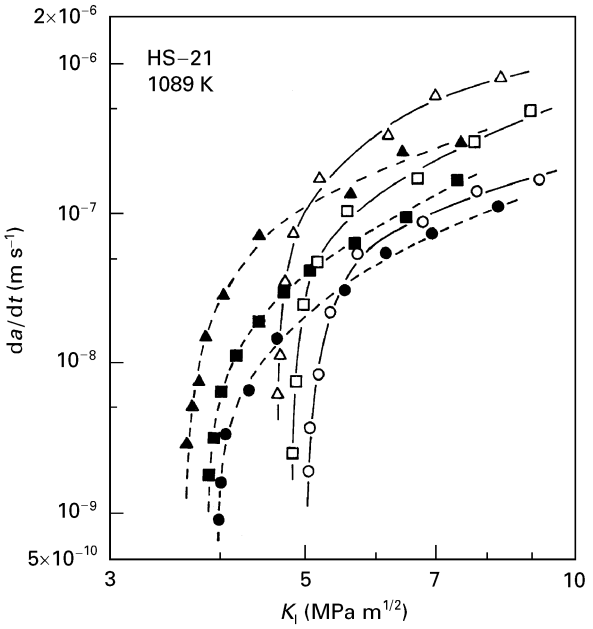


*Figure 12* The relationship between the crack-growth rate, d$a$/d$t$, and the maximum stress intensity factor, $K_I$, in the HS-21 alloy during creep at 1089 K, for $\sigma_g$ = (▲, ■, ●) 73.5 MPa, and (△, □, ○) 88.2 MPa. $D_{gb}$: (▲, △) 1.056, (■, □) 1.162, (●, ○) 1.241.

where $\sigma_g$ is the gross stress. The crack-growth rate (d$a$/d$t$) is lower in the specimens of the higher $D_{gb}$ values, but the difference in the value of d$a$/d$t$ was larger at the smaller $K_I$ values (i.e. in the early stage of the crack growth) between these specimens. The threshold stress intensity factor for crack growth, below which the crack does not grow, is higher in the specimens of the higher $D_{gb}$ values, although it seems to be a little higher under the higher gross stress (88.2 MPa). As described in the previous section, the mean value of the fractal dimension of the grain-boundary fracture, $D_f$, is close to that of the fractal dimension of the grain boundaries, $D_{gb}$, in the smooth, round, bar specimens. Therefore, the crack growth in the microscopic scale may be controlled by the grain-boundary microstructures also in the surface-notched specimens.

Kitagawa and Yuuki [25] have reported that the $K_I$ value of a deflected crack depends on the ratio of the deflected portion of the total length of the crack, and that $K_I$ decreases with increasing proportion of the deflected part of the crack, even for the same projected crack length on the original crack trajectory. Ishida [26] has shown that the $K_I$ value of a serrated crack normal to the tensile axis is almost constant, independent of the number of serrations. Suresh [27] has also obtained similar results and has shown that the circumvention of the crack path by serrated grain boundaries may retard the crack growth by lengthening the crack path. The grain-boundary crack is deflected not only at ledges, bumps, steps or precipitates on grain boundaries but also at grain-boundary triple junctions. The effect of grain-boundary configuration may be reduced by the crack deflection at grain-boundary triple junctions when the length of the grain-boundary crack is more than several grain diameters. Similar results were obtained on the austenitic 21Cr–4Ni–9Mn heat-resisting steel [22]. As shown by

the value of $s_{gb}$, there may be a local variation of the grain-boundary microstructures at the crack front, but this variation may be averaged along the crack front during the crack-growth process. Therefore, the crack growth can be correlated to the mean value of the fractal dimension of the grain boundaries, $D_{gb}$, in each specimen.

## 4. Conclusions

The creep–rupture properties and the initiation and growth of the grain-boundary cracks were investigated using four kinds of specimen of the cobalt-base HS-21 alloy with various grain-boundary microstructures at 1089 K in air. The results obtained were summarized.

1. Both the rupture strength and the creep ductility increased with increasing mean value of the fractal dimension of the grain boundaries, $D_{gb}$, in the specimens. The strain to the initiation of the grain-boundary crack was largest in the specimen of the highest $D_{gb}$ value (1.241), while the strain was much the same in the specimens of the $D_{gb}$ value less than 1.162. This behaviour was explained by the local variation in the grain-boundary microstructures indicated by the standard deviation of the fractal dimension of the grain boundaries, $s_{gb}$.

2. The mean value $D_f$, and the standard deviation, $s_f$, of the fractal dimension of the grain-boundary fracture were, respectively, close to the values of $D_{gb}$ and $s_{gb}$ although the value of $D_f$ was a little higher than the value of $D_{gb}$ in the specimens of the lower $D_{gb}$ values. The creep–rupture properties were correlated to the microstructural features of the grain boundaries and of the grain-boundary fracture surfaces indicated by these fractal dimensions, $D_{gb}$ and $D_f$. The fracture appearance changed from a brittle grain-boundary fracture to a ductile one with increasing values of $D_f$ and $D_{gb}$.

3. The growth rate of the grain-boundary crack was lower in the specimens of the higher $D_{gb}$ values, because the creep crack growth was possibly controlled by the averaged grain-boundary microstructures at the crack front. The effect of the grain-boundary configuration on the crack growth was larger at the smaller $K_I$ value (at the early stage of the crack growth). The threshold stress intensity factor for crack growth was higher in specimens with higher $D_{gb}$ values.


## Acknowledgement

The author thanks Mr M. Kimura, Akita Engineering and Technology Center, for his assistance in the operation of the scanning electron microscope.


## References


1. W. BETTERIDGE and A. W. FRANKLIN, *J. Inst. Metals* **85** (1956–57) 473.
2. M. YAMAZAKI, *J. Jpn Inst. Metals* **30** (1966) 1032.
3. V. LUPINC, "High Temperature Alloys for Gas Turbines 1982" (Reidel, Dordrecht, 1982) p. 395.
4. M. KOBAYASHI, O. MIYAGAWA, T. SAGA and D. FUJISHIRO, *J. Iron Steel Inst. Jpn* **58** (1972) 79.
5. M. YAMAMOTO, O. MIYAGAWA, M. KOBAYASHI and D. FUJISHIRO, *ibid.* **63** (1977) 1848.
6. M. TANAKA, O. MIYAGAWA, T. SAKAKI and D. FUJISHIRO, *ibid.* **65** (1979) 939.
7. M. TANAKA, O. MIYAGAWA, T. SAKAKI, H. IIZUKA, F. ASHIHARA and D. FUJISHIRO, *J. Mater. Sci.* **23** (1988) 621.
8. M. TANAKA, H. IIZUKA and F. ASHIHARA, *ibid.* **24** (1989) 1623.
9. M. F. ASHBY, R. RAJ and R. C. GIFKINS, *Scripta Metall.* **4** (1970) 737.
10. R. RAJ and M. F. ASHBY, *Metall. Trans.* **2** (1971) 1113.
11. F. W. CROSSMAN and M. F. ASHBY, *Acta Metall.* **23** (1975) 425.
12. B. B. MANDELBROT, D. E. PASSOJA and A. J. PAULLAY, *Nature* **308** (1984) 721.
13. V. Y. MILMAN, N. A. STELMASHENKO and R. BLUMENFELD, *Progr. Mater. Sci.* **38** (1994) 425.
14. B. B. MANDELBROT, "The Fractal Geometry of Nature," translated by H. Hironaka (Nikkei Science, Tokyo, 1985) p. 25.
15. M. TANAKA, *J. Mater. Sci.* **27** (1992) 4717.
16. *Idem*, *ibid.* **28** (1993) 5753.
17. M. TANAKA and H. IIZUKA, *Z. Metallkde.* **82** (1991) 442.
18. A. M. GOKHALE, W. J. DRURY and S. MISHRA, ASTM STP 1203, edited by J. E. Masters and L. N. Gilbertson (American Society for Testing and Materials, Philadelphia, PA, 1993) p. 3.
19. W. J. DRURY and A. M. GOKHALE, *ibid.*, p. 58.
20. H. TAKAYASU, "Fractals in the Physical Sciences," (Manchester University Press, Manchester, New York, 1990 p. 11.
21. S. ISHIMURA and S. ISHIMURA, "Fractal Mathematics," (Tokyo Tosho, Tokyo, 1990) p. 246.
22. M. TANAKA, H. IIZUKA and F. ASHIHARA, *J. Mater. Sci.* **23** (1988) 3827.
23. R. H. DAUSKARDT, F. HAUBENSAK and R. O. RITCHIE, *Acta Metall.* **38** (1990) 142.
24. A. KIUCHI, M. AOKI, M. KOBAYASHI and K. IKEDA, *J. Iron Steel Inst. Jpn* **68** (1982) 1830.
25. H. KITAGAWA and R. YUUKI, *Trans. Jpn. Soc. Mech. Eng.* **41-346** (1975) 1641.
26. M. ISHIDA, *Trans. Jpn. Soc. Mech. Eng.* **45-392** (1979) 306.
27. S. SURESH, *Metall. Trans.* **14A** (1983) 2375.



*Received 16 February*
*and accepted 17 September 1996*